International Journal of Fatigue 97 (2017) 177–189

Contents lists available at ScienceDirect

International Journal of Fatigue

journal homepage: www.elsevier.com/locate/ijfatigue

On cold dwell facet fatigue in titanium alloy aero-engine components

M.A. Cuddihy [a,*], A. Stapleton [b], S. Williams [b], F.P.E. Dunne [a]

[a] Department of Materials, Imperial College London, United Kingdom
[b] Rolls-Royce plc, Derby, United Kingdom

ARTICLE INFO

Article history:
Received 19 August 2016
Received in revised form 25 November 2016
Accepted 28 November 2016
Available online 29 November 2016

Keywords:
Cold dwell fatigue
Crystal plasticity
Titanium alloys
Aero-engine discs

ABSTRACT

This paper investigates the mechanisms of facet nucleation through combining aero-engine manufacturer disc component test data with microstructure-sensitive crystal plasticity finite element (CPFE) models. Full-scale component testing has been carried out in a manner representative of in-service conditions. Elastic FE analyses of discs under these conditions and fully accounting for thermal and residual processing strains have also been carried out. Disc facet nucleation sites have been identified and the local stress states evaluated in order to establish crystal plasticity oligocrystal sub-models. The oligocrystal RVE models provide knowledge of hard-soft grain stresses under dwell loading, and the consequent load shedding in order to provide stresses required for the facet nucleation.

The disc component facet observations together with the crystal plasticity sub-model oligocrystal approach provide persuasive evidence that a hard-soft grain combination is required for facet formation, that the remote stress state influences the resolved shear stress on the soft grain initiating slip (with tensile uniaxial stress state more damaging than a tension-tension biaxial stress state), and that the load shedding which results is essential in pushing up the hard-grain basal stress to nucleate facets.

1. Introduction

In-service conditions of an operating gas turbine engine represent some of the most complex loading regimes of any thermo-mechanical system. Titanium alloys are widely used in gas turbine engines, often under extremes of loading, in components such as discs and blades. They are utilised extensively in the aerospace industry due to their low density, excellent corrosion resistance and high fatigue strength [1]. However, it has been well recognised over the past 40 years that titanium alloys suffer from a significant failure mode known as cold dwell fatigue, often characterised by facet crack nucleation and subsequent growth. The lifetime reduction resulting from the inclusion of load holds at maximum stress, and at ambient temperature (<200 °C), during each loading cycle is termed the dwell fatigue life debit. It continues to be a significant industrial concern because its non-destructive evaluation management is hugely costly, and it remains a safety-critical issue. The compressor discs used in the intermediate pressure section of a jet engine are among the components deemed to be 'life-critical', meaning that rupture or failure is not an acceptable outcome due to risk to the airframe integrity; the required reliability for these components is 1 event in 10^8 flights [2].

Considered fundamental to cold dwell fatigue is the formation of facets which are always associated with the failure initiation site. The commonly utilised model for facet nucleation is an adaption of the classical Stroh model for crack initiation due to dislocation pile-up [3], introduced by Evans and Bache [4]. An important subsequent modification to this model included the incorporation of the dwell component, by Hasija and colleagues [5]. The time-dependent stress redistribution, or load shedding, is now believed to be key to the formation of facets and this is recognised in this work. The facet nucleation process occurs on basal planes and is argued to preferentially develop on a grain badly orientated for slip (hard grain), with c-axis near or parallel to the local maximum principal stress direction, adjacent to a soft grain well orientated for slip, be that occurring on prismatic or basal systems. The stress acting normal to the basal plane (and, as some authors argue, the shear stress) during the dwell period, leading to load shedding, is thought to be necessary (but not sufficient) for facet nucleation [6,7].

Evans and Bache [4] were the first to explicitly attempt an investigation of a multiaxial dwell loading regime. They performed tension, torsion, and combined tension-torsion experiments and were able to make a comparison of effective stress at failure and lives-to-failure (N_f). For equal values of Von Mises effective stress, it was observed that tension-torsion tests (i.e. the inclusion of an in-phase shear loading component) often had a higher lives-to-

* Corresponding author.
E-mail address: mitch.cuddihy@imperial.ac.uk (M.A. Cuddihy).

http://dx.doi.org/10.1016/j.ijfatigue.2016.11.034
0142-1123/

failure value than simple uniaxial tension. However, as Doquet and De Greef point out [8], shear loading resulting from torsion is not particularly representative of aero engine in-service conditions so these findings are not directly comparable with the dwell regime. A study carried out by Doquet and De Greef [8] consisted of a series of tests comparing uniaxial and tensile equibiaxial loadings in low cycle fatigue (LCF) and dwell fatigue. The results obtained, while providing valuable insight, were subject to quite considerable scatter, but the indication from the biaxial loading testing in low cycle fatigue was that tensile equibiaxial loading conditions have an ameliorating effect, resulting in extended fatigue life. In many of the dwell fatigue tests performed, the specimens ruptured prematurely, precluding conclusive interpretation. Doquet and De Greef attempted to rationalise their findings in light of the classic multiaxial theories (such as Fatemi-Socie, Sines and Crossland etc.) but found that none of these was able to accurately capture the behaviour observed.

In further LCF (as opposed to dwell) work, Bonnand et al. [9] tested a range of Ti-6Al-4V samples in combined tension-torsion and equibiaxial tension under LCF and found that few of the theories predict, with confidence, observed behaviour. They developed an ad-hoc theory which represents a compromise between the two major categories of multiaxial fatigue criteria; namely critical plane theory and effective stress amplitude. A review of the myriad multiaxial stress theories has been presented by Kallmeyer et al. [10] who conclude that the Findley parameter and the Manson-McKnight model present the most convincing fit in a survey of a large dataset of experimental LCF findings. These data are, however, for low cycle fatigue only and for non- hexagonal close packed (hcp) metals, so not directly applicable in the context of cold dwell fatigue.

In passing, we note that multiaxial stress states are often associated with ductile fracture. Rice and Tracey [11] considered spherical voids and developed a fundamental description of ductile fracture based on void growth and coalescence. The Rice and Tracey model was employed by Helbert et al. [12] who undertook a detailed investigation of the effects of stress triaxiality on the damage mechanisms of an equiaxed α/β Ti-6Al-4V. They found that in the low triaxiality range (values less than 0.66) no significant growth of voids is observed, even up to high plastic strains ($\varepsilon^p < 0.3$). This point has been demonstrated again in more recent work on notched samples of IMI834 by Kumar et al. [13].

The Stroh model is not the only proposed explanation for dwell fatigue in the literature. Lefranc et al. [14] investigated dwell fatigue in Ti-6242 with a bimodal α/β microstructure and argued that crack nucleation was caused by the coalescence of cavities or voids, induced by shear stresses. These voids nucleated at the α/β interfaces and were observed to be greater in size and number under dwell fatigue loading, as opposed to static creep or normal fatigue conditions. Shear induced porosities causing micro cracks under dwell loading were also observed by Gerland et al. [15]. These authors assert that it is the porosities developed under creep conditions of the load hold that are responsible for dwell fatigue, which is in keeping with classic ductile fracture theories [11]. The loading applied to generate this failure mechanism was close to or exceeding macroscopic yield ($\sigma_{0.2\%}$) and the failure may therefore not be mechanistically the same as that occurring at lower in-service stresses in aero-engine discs.

It is known from industrial experience that under in-service conditions the stresses carried by the titanium alloy components (compressor discs) are far lower than yield, at approximately 50–70% of the yield stress. Small-scale laboratory dwell testing is typically found to require much higher stresses in order to induce dwell fatigue failure. Importantly, it is noted that in the majority of cases of failure resulting from dwell fatigue observed in industrial testing, the "worst case" grain orientations are always present (see later). Laboratory samples may consist of relatively small numbers of grains across the gauge section and may not capture the statistics of full-scale components. In such samples, the worst case (rogue) combination of grain crystallographic orientations [16] may simply not be present; a compressor disc contains a volume of material several orders of magnitude larger than that for a simple tensile specimen. The high stresses required to generate facets in the absence of a rogue pair may also be the cause of other undesirable failure states. Bache et al. demonstrate that in the absence of the worst case grain orientation, crack nucleation may be forced onto other combinations, again at high applied stresses [17]. Pilchak et al. [18] found that facets may occur on basal planes, mis-orientated with the macroscopically applied load by approximately 43°. However, this test was also carried out at the relatively high stress of 0.95 σ_y.

This paper presents an investigation on facet nucleation in α-titanium alloy discs from a comprehensive industry spin test programme in such a way to unambiguously avoid the small volume, high stress problem associated with laboratory dwell fatigue testing. We begin by considering the stress states in a rotating disc, establishing the basis for a further in depth study of multiaxial stress loading. This is followed by a detailed examination of stress states and facet nucleation results from disc spin tests carried out by an aero-engine manufacturer. This continuum level study indicates the necessity of a detailed crystal plasticity sub-modelling approach which is used to illustrate the effects of multiaxial stress state on the rogue grain combination and facet nucleation. The nature of the hard grain crystallographic orientation with respect to the principal stress is briefly assessed in the context of experimental observations reported in the literature. The macro-level stress state analysis of the disc is then coupled with the crystal plasticity analyses which allow us to investigate more fully the connection between load shedding and facet nucleation in discs under dwell fatigue. This facilitates prediction of the likely sites of facet nucleation and the stress levels and states necessary to cause them.

2. Disc spin test studies

2.1. Introduction to spin tests

In the absence of predictive capabilities due to the complexities of structure, texture and properties, aero-engine manufactures have had to rely on an expensive (>£150,000 each) set of time-consuming (5–8 weeks per test) spin tests to establish a reliable applied stress-to-life (S-N) curve [2]. Spin tests are a form of quality control which involve taking full sample discs manufactured as standard product hardware with fully representative geometric features, which are cycled in a manner similar to in-service use, often until failure.

Rolls-Royce have undertaken a comprehensive spin test programme for a variety of in-service components and one particular set of results is examined here. This set is defined as a series of spin tests of discs, tested to failure, from the same forging and with the same geometry.

The illustration in Fig. 1(a) shows a 3D rendering of the disc using the geometry supplied by the manufacturer (with a 1/4 cut-away for clarity). The inset figures illustrate an axisymmetric slice of the disc and show the facet locations. These facet locations, identified by the black spots in the bore region, have been measured and quantified as the failure origins for the various dwell cycle tests. These sites are collectively similar, such that they represent the qualities associated with classical facet behaviour seen in dwell fatigue, i.e. basal plane orientation approximately perpendicular to the principal stress direction (hoop), and quasi-cleavage fracture planes.

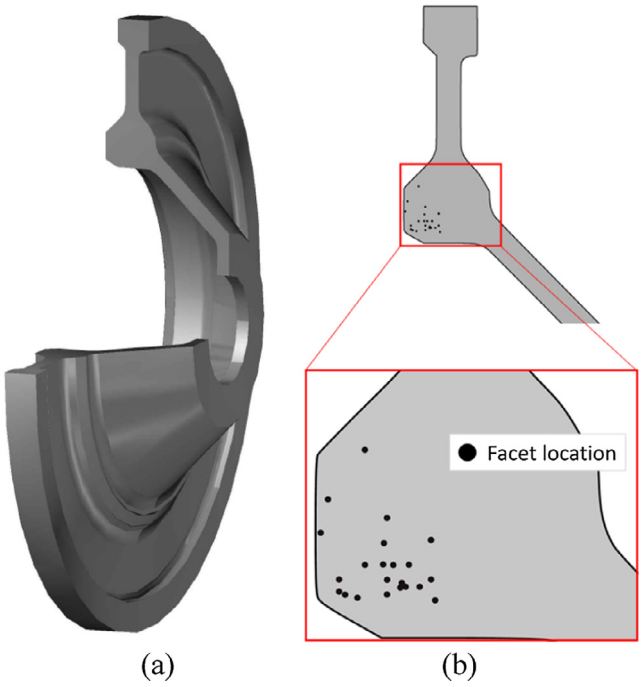

Fig. 1. Compressor disc geometry from spin tests, (a) cutaway of a 3D rendering of a disc, and (b) axisymmetric slice of disc highlighting the key bore region with facet locations.

2.2. Stress distributions in compressor disc spin tests

An axisymmetric finite element (FE) model with isotropic, elastic material properties representing the compressor disc material (an α-Ti variant, Ti-834) is utilised to determine stress states for disc spin tests. The model replicates the spin test temperature (<200 °C, known to be the range conducive for dwell) and assumes an isothermal state. Interestingly, a temperature of 120 °C is argued to be the worst case for dwell fatigue [19]. The model is loaded to replicate the typical cycling of the spin test, i.e., rotational loading at minimum RPM and spinning up to a peak rotational speed which is held for 2 min (dwell condition), after which the speed is reduced back down to the idle condition.

Prior to spin loading, an initial step is carried out to include the residual stresses developed by the post-forging heat treatment, aging, and quenching operations. The thermal strains generated by the quenching process are calculated in a separate model of the bulk forged element, and the resulting strains are mapped onto the rig test model. The calculation of the thermal strains induced by the quenching process is verified against a measurement of the strains by an incremental hole-drilling test.[1] This involves bonding standard copper strain gauges to the specimen, then drilling a hole through the strain gauge and the material. As the material relaxes around the hole, the displacements measured by the strain gauge can be used to back calculate the surface residual strains [20]. This technique is only suitable for near-surface measurements of strain. Alternative methods of measuring the process residual strains at depth have been developed using synchrotron X-ray diffraction; this technique has been used to measure residual strains in nickel superalloy turbine discs and may probe up to ~50 mm beneath the surface [21].

The contour plots in Fig. 2 show the principal normalised stress distributions, corresponding to the hoop, radial and axial stress directions respectively (there are minimal amounts of shear observed in these models) at full spin loading, and including the initial residual stresses. These operating stresses have been normalised by a representative tensile strength. Fig. 2 also shows three representative facet locations.

Evidently, the hoop stresses dominate over the other two directions, and the peak concentrations are localised in the lower left region of the disc bore. However, relatively large radial stresses are carried by the diaphragm section of the disc where the radial stress is almost 40% of the hoop stress for that region.

Fig. 3 shows a close up and more detail of the hoop stresses with respect to the 22 experimentally observed facet nucleation sites. An immediate observation is the strong dependence on the hoop stress i.e. no faceting is observed to occur when the normalised hoop stress is less than 0.58 with the majority of facets occurring at hoop stress values greater than 0.66.

A simple design paradigm may be to assume that peak hoop stress is the dominant driver of facet nucleation, but the facet outliers (e.g. a13, a1) cannot be explained in this way. In addition, why is there just the one observed facet location on the 0.58 stress contour? For completeness, this is examined further at the continuum level by determining the stress triaxiality ratio for the bore region, which is shown in Fig. 4. The stress triaxiality χ, is the ratio of the hydrostatic mean stress and the von Mises effective stress given by

$$\sigma_H = 1/3(\sigma_1 + \sigma_2 + \sigma_3) \tag{1}$$

$$\sigma_e = \frac{1}{\sqrt{2}}\sqrt{(\sigma_1 - \sigma_2)^2 + (\sigma_2 - \sigma_3)^2 + (\sigma_3 - \sigma_1)^2} \tag{2}$$

$$\chi = \sigma_H/\sigma_e \tag{3}$$

Fig. 4 shows that the facet nucleation locations fall within a quite tight banding of triaxiality ratio, with average triaxiality of ~0.34, which represents an approximately uniaxial tensile stress state. The facet point a13, previously considered an outlier with respect to hoop stress, is now observed to have the same stress triaxiality as the majority of the other facet locations.

However, other bore locations with equivalent triaxiality values on the right-hand side of the bore section (indicated in Fig. 4) do not show any incidences of facet nucleation such that a triaxiality of $\chi = 0.34$ is clearly not a sufficient condition for faceting. Finally, in contrast with the earlier discussion on stress triaxiality related to laboratory specimens, high (tensile) triaxiality is definitively not associated with dwell facets. The highest value of χ, 0.55, is far removed even from the closest facet location, a13. It is important to note that the operating stresses in the bore region are *much* lower than the $\sigma_{0.2\%}$ yield stress, such that classical multiaxial continuum stress theory or ductile fracture models are simply not relevant. Hence, the next section seeks to provide mechanistic understanding through the use of crystal plasticity sub-models which replicate the location-specific crystallography, stress states and load shedding resulting from the spin test loading.

3. Crystal plasticity modelling of biaxial loading in dwell fatigue

The previous section demonstrated that multiaxial stress states develop within the disc, and that while the hoop stress due to rotational speed is large, it is not the sole component of stress. Doquet and DeGreef's work [8] indicates that equibiaxial tensile loading may have a positive effect on fatigue life, as opposed to uniaxial tension. Secondly, the torsion testing work by Evans and Bache [4] demonstrates that shear loading affects fatigue life, however it is not a directly representative loading for disc components, so it will not be considered further. Finally, the examination of disc spin data above suggests a link to the multiaxial nature of the stress state. Hence, an approach is presented based on crystal

[1] The residual strain calculation was carried out at Rolls-Royce plc.

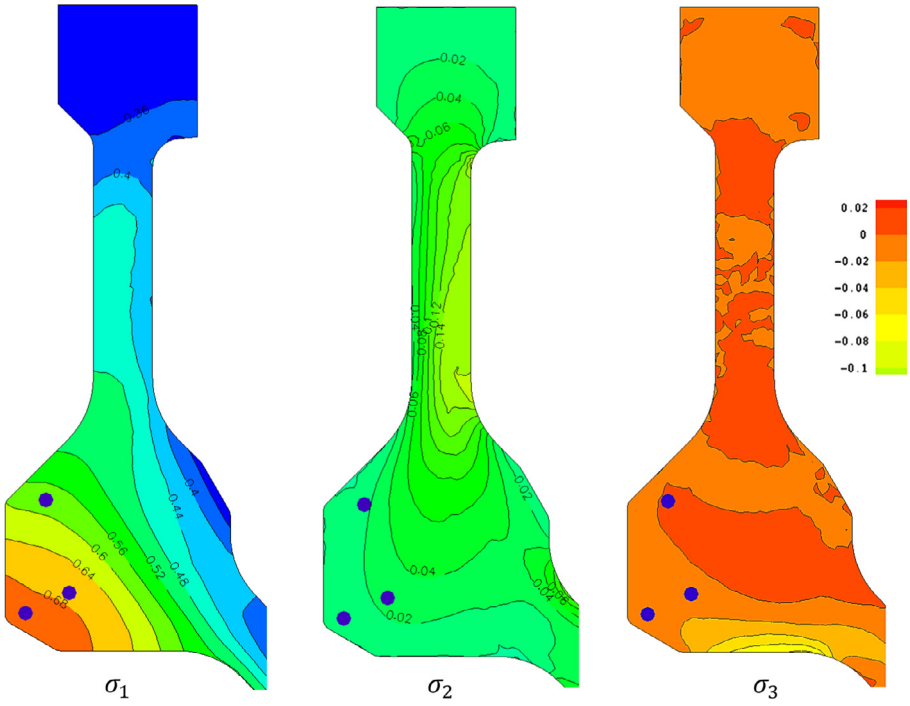

Fig. 2. Distributions of normalised hoop (1), radial (2) and axial (3) principal stresses; values indicated on the isolines (except for σ_3). Example facet nucleation sites shown by blue circles. (For interpretation of the references to colour in this figure legend, the reader is referred to the web version of this article.)

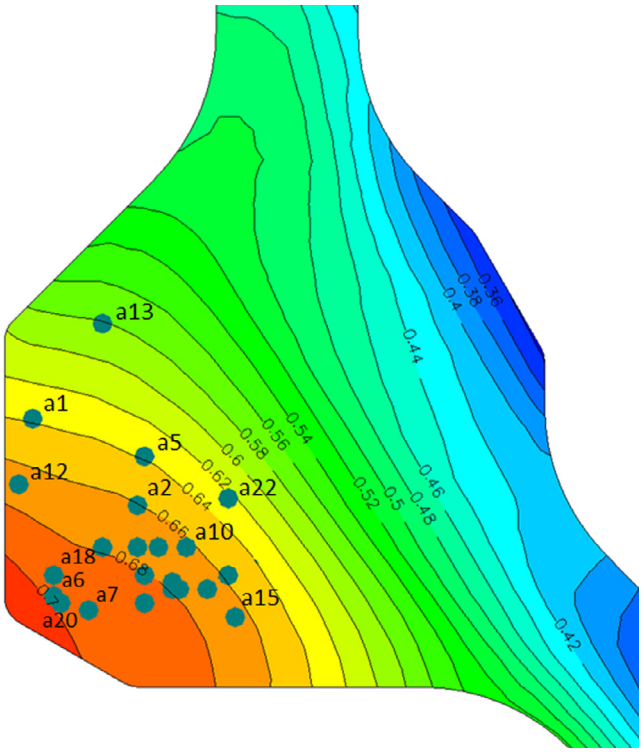

Fig. 3. Detailed assessment of facet location sites with respect to normalised hoop stress distribution, with some facet locations labelled.

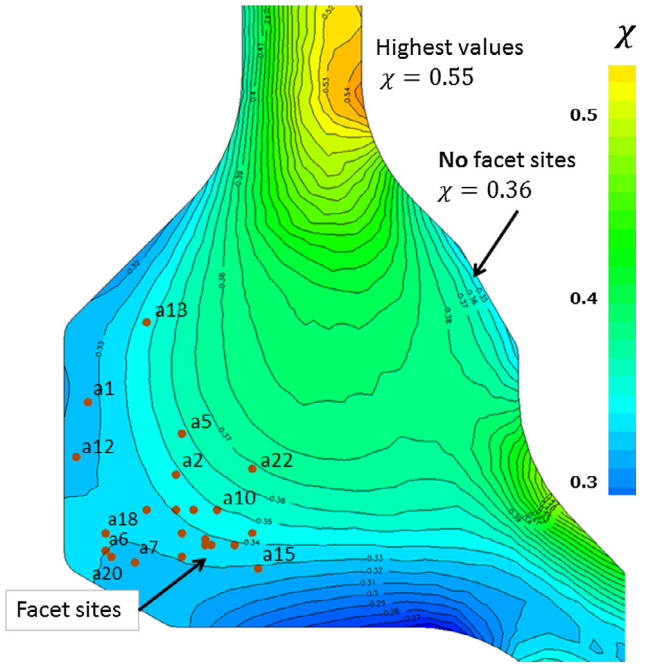

Fig. 4. Bore section contour plot showing stress triaxiality and facet nucleation locations.

plasticity sub-modelling which provides the link between facet nucleation at the microstructural level with the continuum disc stress states developed under in-service loading. With knowledge of the facet nucleation sites within the spin tested discs, the macroscale stress states determined above at these locations are imposed at the sub-model crystal plasticity level, as indicated schematically in Fig. 5.

For each facet nucleation site, a multigrain representative volume element (RVE) is developed, each of which contains the classical hard-soft grain orientation combination conducive to dwell load shedding. The macroscale stress state at each facet location is extracted from the disc analysis above and imposed locally at the sub-model crystal plasticity level. However, before presenting

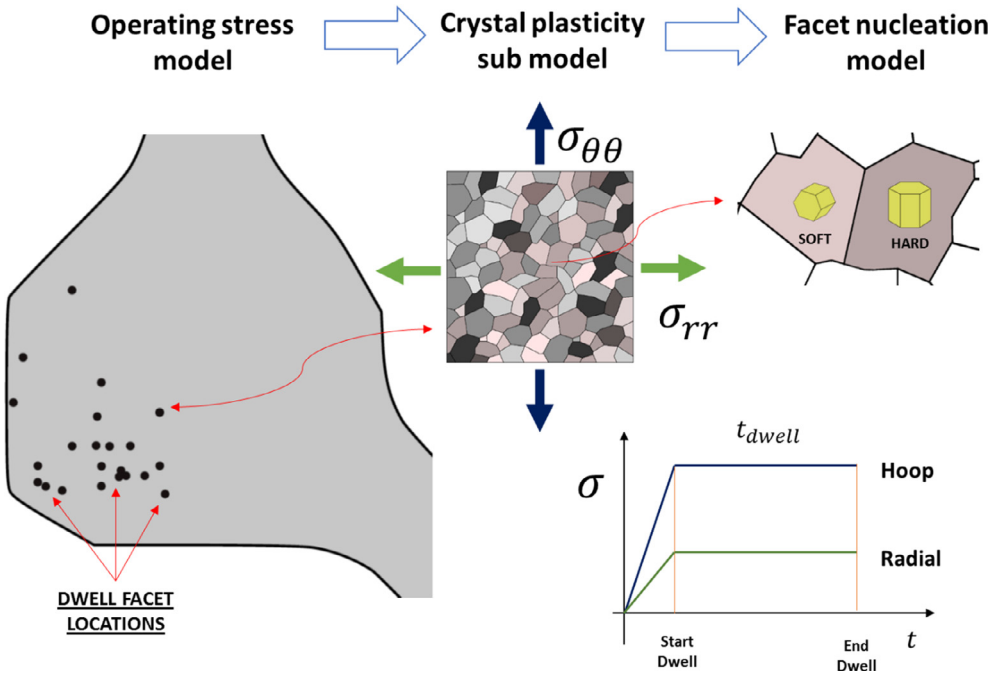

Fig. 5. Schematic of sub-modelling procedure to calculate facet stress state.

disc facet nucleation results, we briefly discuss the crystal plasticity framework utilised in the analyses, and carry out systematic studies of the role of biaxial stress states in load shedding, and the effect of the orientation of the hard grain.

3.1. Crystal plasticity framework

The rate-dependent crystal plasticity framework utilised in this study is based on that originally developed by Dunne et al. [22]. We begin by stating that the multiplicative kinematic decomposition of the deformation gradient ($\boldsymbol{F}$), into elastic ($\boldsymbol{F}^e$) and plastic ($\boldsymbol{F}^p$) tensors is given by Lee [23] such that:

$$\boldsymbol{F} = \frac{\partial \boldsymbol{x}}{\partial \boldsymbol{X}} = \boldsymbol{F}^e \boldsymbol{F}^p \tag{4}$$

Assuming crystallographic slip accounts for plastic deformation, and for now considering just single slip,

$$\boldsymbol{F}^p = \boldsymbol{I} + \frac{\partial \boldsymbol{u}^p}{\partial \boldsymbol{X}} = \boldsymbol{I} + \gamma(\boldsymbol{s} \otimes \boldsymbol{n}) \tag{5}$$

in which $\boldsymbol{s}$ and $\boldsymbol{n}$ are slip direction and plane normal respectively, and γ is the magnitude of the slip. Since the material properties at a point are time-dependent, it is convenient to write the plastic deformation gradient in rate form as

$$\dot{\boldsymbol{F}}^p = \dot{\gamma}(\boldsymbol{s} \otimes \boldsymbol{n}) \tag{6}$$

For a spatially varying velocity field, the velocity gradient is defined and decomposed into the symmetric and anti-symmetric parts as

$$\boldsymbol{L} = \dot{\boldsymbol{F}}(\boldsymbol{F})^{-1} = sym(\boldsymbol{L}) + asym(\boldsymbol{L}) = \boldsymbol{D} + \boldsymbol{W} \tag{7}$$

where $\boldsymbol{D}$ and $\boldsymbol{W}$ are the deformation rate and spin tensors, respectively. Both $\boldsymbol{D}$ and $\boldsymbol{W}$ may be further decomposed into elastic and plastic parts as:

$$\boldsymbol{D} = \boldsymbol{D}^e + \boldsymbol{D}^p \tag{8}$$

$$\boldsymbol{W} = \boldsymbol{W}^e + \boldsymbol{W}^p \tag{9}$$

The rate of crystal plastic deformation is

$$\boldsymbol{D}^p = sym(\boldsymbol{L}^p) \tag{10}$$

and the plastic spin

$$\boldsymbol{W}^p = asym(\boldsymbol{L}^p) \tag{11}$$

The plastic velocity gradient is that associated with plastic flow through a fixed lattice, including contributions from all slip systems, and is given by

$$\boldsymbol{L}^p = \sum_{i=1}^{n} \dot{\gamma}^i \boldsymbol{s}^i \otimes \boldsymbol{n}^i \tag{12}$$

with normal vectors $\boldsymbol{n}^i$ and slip direction vectors $\boldsymbol{s}^i$ corresponding to the ith slip system. The slip rate, $\dot{\gamma}^i$, is computed according to a slip rule, described next.

Dislocation pinning is taken to occur through the presence of lattice obstacles, which may include solute atoms, the sessile statistically stored dislocations (SSDs) and their associated structures, as well as geometrically necessary dislocations (GNDs), incorporated in the slip rule as an overall obstacle density. The resultant slip rule (defined explicitly in Dunne et al. [22]) determining the slip rate of a given slip system takes the form:

$$\dot{\gamma}^i = \begin{cases} 0, & |\tau^i| < \tau_0 \\ \rho_s^m b^{i^2} v \exp\left(-\frac{\Delta F}{kT}\right) \sinh\left(\frac{(|\tau^i| - \tau_c^i)\Delta V^i}{kT}\right), & |\tau^i| > (x + \tau_0) \end{cases} \tag{13}$$

in which ρ_s^m is the mobile SSD density, ρ_0 the initial sessile dislocation density, b^i the Burgers vector magnitude for slip system i, v the frequency of attempts (successful or otherwise) by dislocations to jump the energy barrier, ΔF the Helmholtz free energy or activation energy, k the Boltzmann constant, T the temperature in Kelvin (K), τ^i the resolved shear stress, τ_c critical resolved shear stress, γ_0 the shear strain that is work conjugate to the resolved shear stress, and ΔV the activation volume, $\Delta V^i = \gamma_0 l b^{i^2}$, where $l = \frac{1}{\sqrt{\rho_0}}$.

The density of sessile statistically stored dislocations is allowed to accumulate in proportion to the accumulated slip, p with

hardening factor, γ', chosen to ensure the experimentally observed hardening is reproduced.

$$\dot{\rho}_{SSD} = \gamma' \dot{p}$$
$$\rho_{SSD}^{t+\Delta t} = \rho_{SSD}^{t} + \dot{\rho}_{SSD}\Delta t \tag{14}$$

This simple relation, with only one parameter, is chosen as it allows for adequate representation of experimental data. It is well understood that SSD evolution is a function of plastic slip, however, the precise nature of this relationship is less clear (and likely varies with temperature, strain rate, and material system). There remain limited quantitative experimental techniques and studies of the SSD evolution with strain, as opposed to GNDs where EBSD based methods have shown excellent results [24,25]. We argue that incorporation of a more complicated evolution rule (such as the Kocks-Mecking rule) with additional fitting factors for dislocation density without further mechanistic understanding does not add much value. GNDs are not directly considered in this work as the average grain size in this study is considered to be ~500 μm likely representative of the effective structural unit size of the industrial material with respect to dwell fatigue; in this context effective structural unit is analogous to the microtextured region referred to in other studies, such as [18]. Previous experimental studies have shown that length scale effects and strain gradient associated dislocations are likely to be significant for much smaller length scales (<50 μm) [26].

Each slip system becomes active when the resolved shear stress is equal to or greater than the combined effects of the back stress and the size-independent critical resolved shear stress ($|\tau^i| \geqslant \tau_0$). The back stress on a slip system is described by the following relation:

$$x^i = \alpha G b \sqrt{\rho_{total}} = \alpha G b \sqrt{\rho_{GND} + \rho_{SSD}} \tag{15}$$

Note that: $\alpha = \frac{1}{\pi(1-\nu)}$, and which is approximately 0.5 for titanium.

The crystal model is implemented within a combined Abaqus user-defined element (UEL) [27], which facilitates strain gradient calculations, and user defined material property (UMAT) subroutine.

3.2. Material calibration of slip rule

This work focuses on the cold dwell susceptible, near-alpha phase, titanium alloy Ti-6Al which is hexagonal close packed (hcp), and has 24 slip systems. It is assumed that there is no twinning and that crystallographic slip is the only source of inelastic deformation [1]. The ⟨*a*⟩ and ⟨*c*+*a*⟩ type systems are differentiated (*c*/*a* ratio of 1.587 is used), and the slip systems for a single hcp crystal are shown in Fig. 6.

Hasija et al. [5] conducted mechanical tests with samples of single-phase α-Ti–6Al, for both single crystal and polycrystalline samples. The single crystal tests were carried out at constant strain rate, for basal and prismatic slip ⟨a⟩, and pyramidal slip ⟨c+a⟩, and the stress strain curves generated by these tests when coupled with a CPFE single crystal model allow us to establish the base critical resolved shear stresses, see Fig. 7(a). Also, as hardening is hardly observed in the tests, the hardening coefficient γ' in the SSD hardening rule is set to a small non-zero value of 0.05. Equal strengths are assumed here for basal and prismatic ⟨a⟩ slip systems for simplicity, since the difference between them has been observed to be small in the experiments of Hasija et al., as well as the micro cantilever experiments of Gong et al. [28]. However, it is noted that in some reported studies in the literature, variance is observed in the values of the critical resolved shear stress of the basal and prismatic systems.

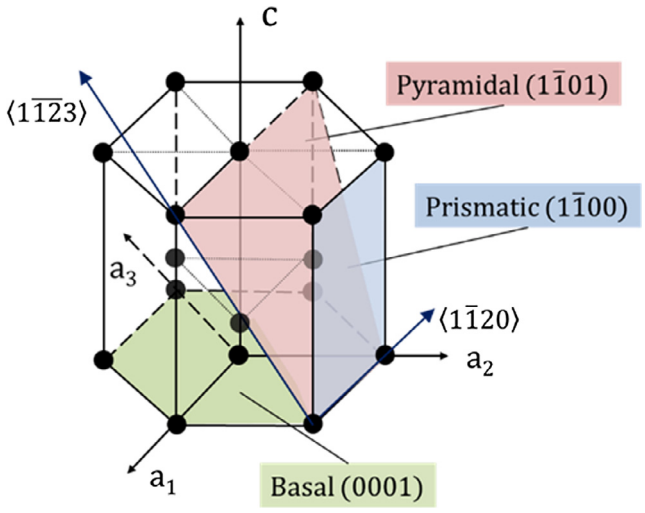

Fig. 6. Hexagonal close packed slip systems for α-phase titanium.

The slip strength of pyramidal ⟨c+a⟩ systems is often observed to be about three times that for basal or prismatic systems, recently demonstrated experimentally by Gong et al. [28].

The polycrystal experiments considered a compression test of three samples at three strain rates, 8.4×10^{-4}, 1.5×10^{-4} and $1.68 \times 10^{-5}\ s^{-1}$, and have been used in combination with a representative polycrystal CPFE model [19] to determine the activation energy, ΔF, relating to strain rate sensitivity (see Eq. (13)). The polycrystal model with a chosen activation energy of $\Delta F = 9.913 \times 10^{-20}$ J/atom is shown alongside the three experimental strain rates indicated in Fig. 7(b), providing a good representation of the polycrystal average stress-strain response. The activation volume is established to be ~18b^3, which is consistent with Conrad's [29] range of values for α-Ti; ~8 to 80b^3.

The small amount of strengthening observed is captured simply by means of the contribution from grains badly orientated for slip within the polycrystal, such that the hardening factor, γ' remains as would be expected from the single crystal tests. Latent hardening is considered for the polycrystal models such that hardening on the *i*th slip system increases the slip strength of all other systems (incorporated in the slip rule via Eq. (15)). Elastic moduli (from Hasija et al. [5]) and all the derived slip rule properties for the representative Ti-6Al alloy are given in Table 1.

These derived slip rule constants have been utilised in a previous study, carried out by some of the authors, on the temperature sensitivity of cold dwell fatigue [19]. CPFE polycrystal models employing these slip rule parameters have been shown to accurately predict the well-known "switching off" of the dwell effect for temperatures in excess of ~200 °C [19].

3.3. CPFE modelling of biaxial dwell stress states

We consider a representative hcp polycrystal sample with fixed in-plane ligament width of 8000 μm and height of 7500 μm, comprising 240 grains. This model is subject to a combination of loads used to represent the two major stress components as observed from the disc operating stress model and indicated in Fig. 8(a). The lateral load, referred to as the secondary load, is representative of the radial stress and is applied in-phase with the primary vertical load – representing the hoop stress. By testing a range of loadings from uniaxial to full equibiaxial states, we can demarcate precisely the influence of the additional load component on the dwell condition.

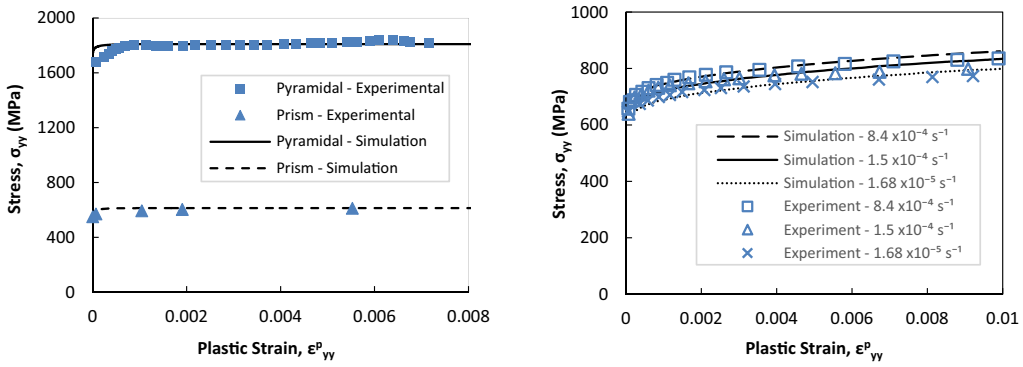

Fig. 7. (a) Experimental and CPFE model curves for prismatic ⟨a⟩ and pyramidal ⟨c+a⟩ slip system response based on single crystal creep experimental data from Hasija et al. [5], and (b) Polycrystal strain rate sensitivity calibration results, experimental data also from Hasija et al. [5].

Table 1
Material property data for Ti-6Al.

Slip rule properties	Value	Elastic constants	Value
ρ^{SSD}_{mobile}	5.0 μm^{-2}	E_{xy}	85 GPa
$\rho_{initial}{}^{SSD}$	0.01 μm^{-2}	E_{yz}	120 GPa
$\rho_{initial}{}^{GND}$	0.0 μm^{-2}	υ_{xy}	0.46
υ	1.0×10^{11} Hz	υ_{yz}	0.22
b ⟨a⟩	3.2×10^{-4} μm	G_{xy}	29 GPa
b ⟨c + a⟩	5.1×10^{-4} μm	G_{yz}	40 GPa
ΔF	9.913×10^{-20} J		
k	1.381×10^{23} J K^{-1}		
T	293 K		
ΔV	18 b^3		
γ'	0.05		

This study addresses microstructural quantities thought to be the most sensitive indicators of local behaviour. Particularly, we consider a combination of two grains buried within the polycrystal orientated such that one is favourable for slip and the other is not; this grain couple is indicated in Fig. 8(b) and is where key stress magnitudes are extracted for analysis. Furthermore, grains have a directionally solidified structure and rectangular morphology, giving prismatic grains, and all grains have the same depth in the out of plane direction. Consideration is given to mesh refinement in the region local to the hard/soft pair with 768 elements per grain, whereas the mesh for the other grains is relatively coarse.

The nature of 'realistic' grain morphology has been addressed by Sauzay and co-workers [30], who have found that it contributes little to the overall mechanistic behaviour with respect to the enormous computational expense in mesh generation, thus motivating the use of simple geometry. Furthermore, as we consider only pure α-phase Ti-6Al alloy, we are not explicitly addressing the β-phase in this study nor α–β morphology effects. The latter are likely to be important for some alloys (eg Ti-6246) and may well have the effect of inhibiting load shedding and dwell. However, we do not consider such systems in this paper. Recent work by Zhang et al. [31] has shown that in micro pillar deformation studies, the

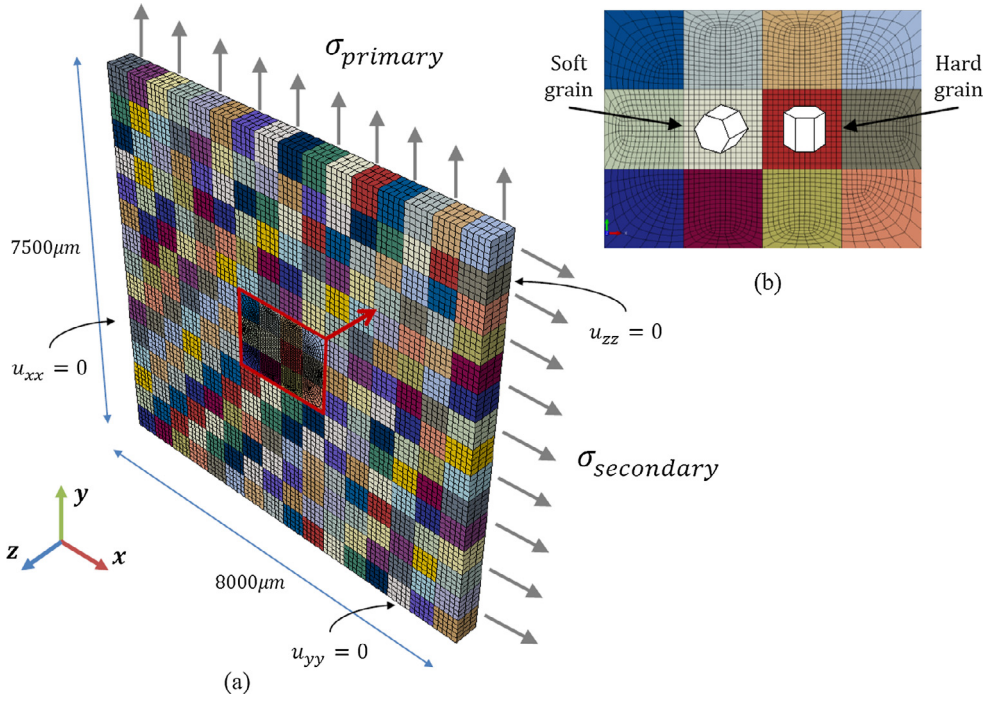

Fig. 8. CPFE polycrystal model: (a) polycrystal model, and (b) the region surrounding the rogue grain pair.

β-laths show some but limited resistance to slip transfer, such that for globular and α–β lath structured grains, the simplified modelling approach is appropriate.

Apart from the hard/soft grain couple with specific misorientation, all other grains in the model are assigned pseudo-random orientations, but with the imposed constraint of having c-axes inclined perpendicularly to the primary remote loading direction (within ±10°) in order to favour easy slip.[2] Pseudo-random here refers to the generation of Euler angles via a random number generator. The material properties and slip rule constants are those described in §3.2.

We examine the results of a systematic study of the effects of the addition of a secondary applied stress, increasing from 0 to 700 MPa; that is, from purely uniaxial to equibiaxial loading. Therefore, each analysis has a fixed primary load of 700 MPa, in the yy-direction, with a differing secondary load, in the xx-direction, from 0 to 700 MPa. These loads are reached after 12 s and held for a dwell period of 120 s. It is during the dwell that stress redistribution potentially occurs from the soft grain to the adjacent hard grain (the load shedding), and in this study, the biaxiality of the stress state and its influence on the load shedding is examined. One typical dwell cycle is chosen for analysis, largely for reasons of computational efficiency, while noting however that there is anecdotal and some physical evidence, which posits that damage may occur in the first cycle of loading, and evolve slowly in subsequent cycles [19].

We choose a point in the hard grain, just inside the boundary with the soft grain and examine the stress in the yy-direction. In this study the hard grain is orientated such that the c-axis is parallel with the primary load and the hcp unit's basal plane is therefore perpendicular to this stress. Therefore we refer to this stress as the 'basal stress' σ_{basal}.

The results shown in Fig. 9(b) demarcate clearly the differences arising from the various load histories for the differing stress states. Firstly, we note the disparity between the two extreme cases for which it is seen that after a two minute dwell period, the difference in stress accumulated by the hard grain is almost 350 MPa. Focusing on the uniaxial load, we see that at the end of the dwell period the basal stress is approximately 1150 MPa, which is close to the commonly accepted value for tensile failure in representative titanium alloy with strong hcp c-axis crystallographic texture. The results compare qualitatively with the work of Doquet and DeGreef which suggests that equibiaxial loading in dwell fatigue would show longer fatigue life. This may be understood from the crystal plasticity model through the apparently far lower accumulation of residual stresses in the hard unit from cycles of equibiaxial dwell loads, as opposed to uniaxial loading. The results in Fig. 9(b) are utilised further in the disc spin test discussion presented later.

3.4. Effect of hard grain orientation with respect to principal loading axis

It has been well established, through experimental observation, that facet fatigue nucleation is almost always associated with fracture on a basal plane which is normally orientated perpendicular to the applied loading. However, several studies have shown that facets can often be upwards of 10–15° in misalignment with the principal stress direction [31]. The figures below show a series of polycrystal analyses in which the hard grain c-axis is rotated from its hardest orientation, parallel to the applied stress, to perpendicular to the applied stress. These analyses are stress hold tests, with uniaxial loading only. We first consider the distribution of accumulation of plastic slip in the region close to the soft/hard pairing.

When the hard grain is aligned parallel with the applied stress as in Fig. 10(a), we see the development of strong slip bands around the hard unit and even a shielding effect is provided for by the hard grain, just below and to the right. Plastic strain development is progressive and preferential, and this is demonstrated by the intensity of the slip bands. The hard grain is rotated by 30° in (b) and by 45° in (c) and with this rotation, a diminution of the intensity of the slip bands around the grain may be seen with some slip activity occurring at the grain boundary of the now former hard unit. When the hard grain is rotated through to 90° the former direction, it is seen to carry plastic strain. This allows for slip bands to form through the rotated hard unit and for plastic strain to be generated in the formerly shielded region.

As dwell facets are always characterised by the stark anisotropy between soft and hard grains, it is of interest to investigate the stress on the basal plane as a function of hard grain orientation, which is considered next. The stress normal to the basal plane illustrated in Fig. 11 is given in terms of the traction and the normal direction by:

$$\sigma_{basal} = (\boldsymbol{t} \cdot \boldsymbol{n}) = (\boldsymbol{\sigma n}) \cdot \boldsymbol{n} \tag{16}$$

in which $\boldsymbol{n}$ is the slip plane normal vector for the particular orientation of the hcp crystal. The rotation of the hard grain from the 'hard' orientation (parallel to the principal tensile load) to the 'soft' orientation (perpendicular to the load) is indicated by the diagram in Fig. 12(b).

Fig. 12(a) shows the effect of hard grain orientation with increasing biaxial stress ratio ($\sigma_2/\sigma_1 \rightarrow 1$). These stress values are for the consistent location in the hard grain and are taken at the end of a 12 s load hold. It is observed that increasing the biaxiality reduces the stress not only for the hardest orientation, but also for the intermediate configurations (i.e. $\theta = 5^\circ$ to $\theta = 20^\circ$) also.

Fig. 12(b) shows the effect on basal stress of rotating the hard grain through 90° under uniaxial loading conditions; interestingly the stress on the basal plane remains relatively flat until an orientation of about 15–20°, after which it falls off considerably. This finding may explain why facets may be found on basal planes which are not uniquely normal to the principal stress direction but often orientated away from this axis, as significant normal basal stresses may be developed for c-axis orientations up to 20° off the principal stress direction.

4. Analysis of disc component results: combining CPFE modelling with spin test studies

In this section, we return to the sub-modelling approach developed above and shown in Fig. 5 in order to link microstructural aspects of facet nucleation with the disc component spin test results. For context, the dependence of single crystal resolved shear stresses on biaxial stress states is considered first and is followed by an assessment of the resolved shear stresses acting on prism slip systems in a hard-soft grain combination located at each of the experimentally observed facet nucleation sites in the spin test data. The sub-modelling approach is presented next in which each spin disc facet location is represented by an oligocrystal containing the hard-soft grain combination subjected to the local disc multiaxial stress state and dwell loading. The consequences of the stress state, the dwell, and the presence of a hard-soft grain combination on stress redistribution, load shedding, and basal stresses on the hard grain are all assessed in the light of the nucleation of facets at these corresponding locations in the disc spin data.

A single crystal is considered first, orientated with respect to the biaxial stress state shown in Fig. 13. The resolved shear stress is

[2] Euler angles will be in the set: $(\phi_1, \phi, \phi_2) = (\phi_1 = 0, -10 < \phi < 10, -360 < \phi_2 < 360)$.

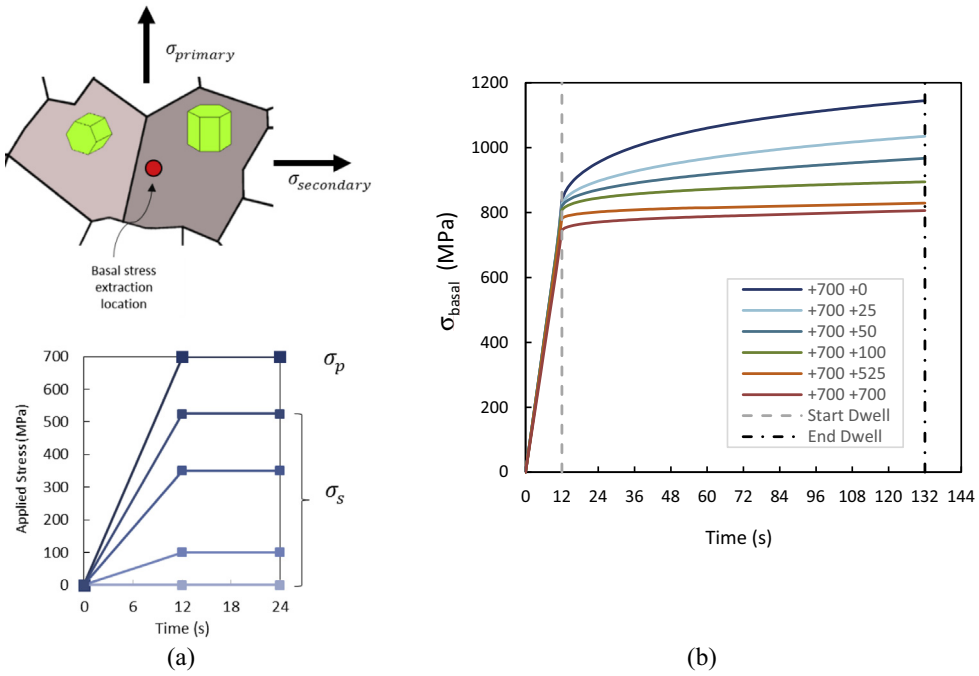

Fig. 9. (a) Range of various load histories with in-phase primary (σ_p) and secondary (σ_s) loads, (b) σ_{basal} for a point inside the grain boundary of the soft/hard grain across loading period (as indicated in the schematic).

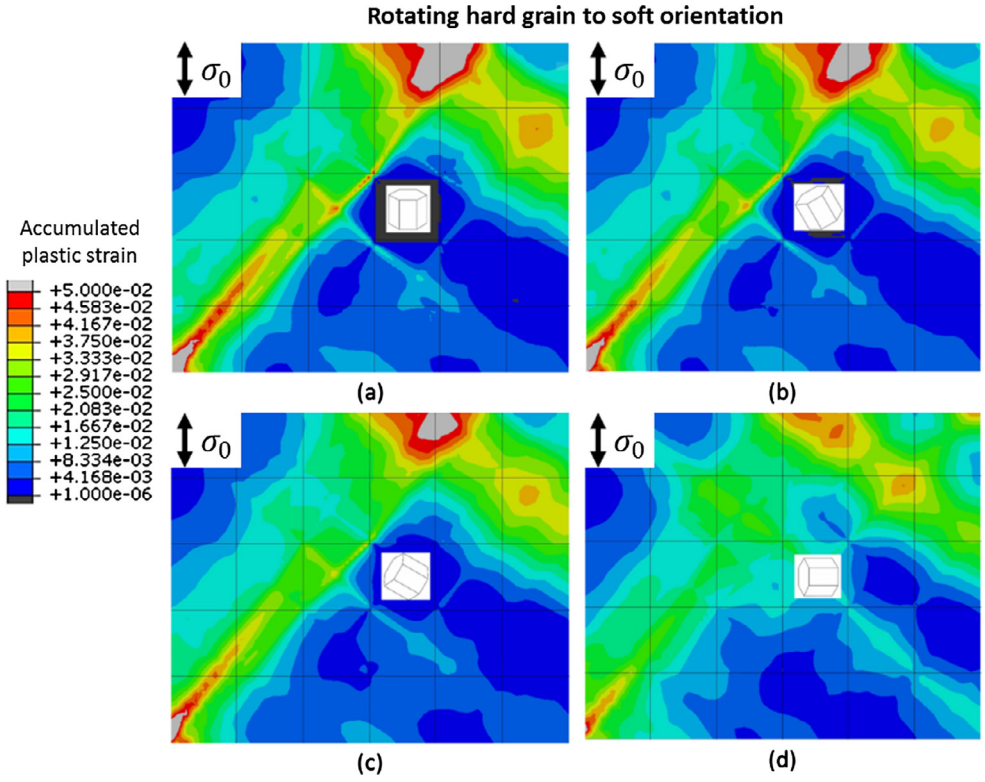

Fig. 10. Accumulated plastic strain contour plots, (a) to (d), for various rotations of the hard grain, from 0° to 90° with the direction of loading indicated.

calculated (simply by applying Schmid rule $\tau_{rss} = \boldsymbol{\sigma n} \cdot \boldsymbol{s}$) on all active slip systems and the highest value (normalised with respect to the threshold value for Ti-6Al) is shown against the biaxial stress ratio (i.e. the ratio of the two orthogonal stresses, $\sigma_2/\sigma_1 = 0$ corresponding to uniaxial loading and $\sigma_2/\sigma_1 = 1$ to equibiaxial loading).

The single crystal is loaded with an increasing lateral load, and a fixed primary load. From Fig. 13 it is clear that with increasing biaxiality the resolved shear stress on the soft grain prism system decreases. Naturally, the imposed biaxial stress state affects the plasticity of initiation of slip in the soft grain, which in a

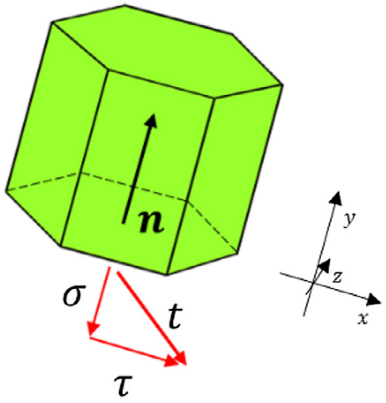

Fig. 11. Typical hexagonal close packed unit under arbitrary traction.

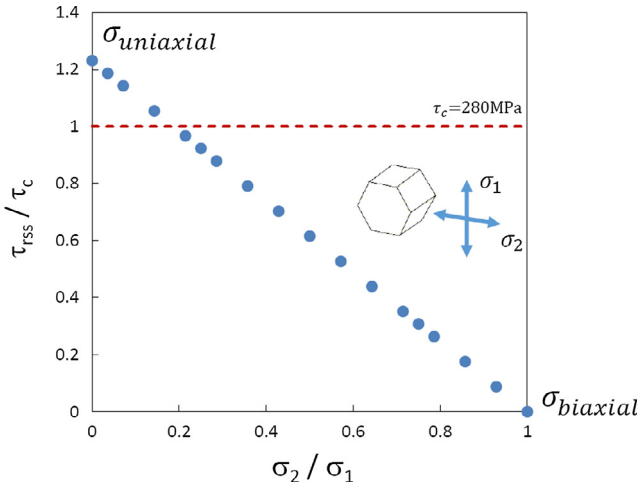

Fig. 13. Normalised single crystal resolved shear stress as a function of principal stress ratio.

soft-hard grain combination is what is required to drive load shedding under dwell fatigue conditions. The absence of slip in the soft grain precludes stress redistribution to the hard grain.

Returning to the compressor disc geometry in Fig. 1, the stress state at each facet nucleation site is extracted and used to determine the resolved shear stress which would develop on a prism slip system occurring at that same location, on the basis that it is known that a soft-hard grain combination (with respect to the disc hoop stress direction) exists at each facet site in the disc. For the purposes of visualisation, the same calculation is carried out everywhere in the disc section, and the corresponding resolved shear stresses developed are shown in Fig. 14.

This rather simple approach, which recognises the role of the hard-soft grain combination for facet nucleation, and takes full account of the stress state in determining the resolved shear stress on the soft grain prism slip system, provides a rational demarcation of the disc regions in which facets are seen to nucleate and those in which they are not, and the demarcation is given by a normalised resolved shear stress of $\tau_{RSS}/\tau_c = 1.0$ where $\tau_c = 280$ MPa. Compared directly with the disc bore triaxiality distribution of Fig. 4, it may be seen that the region to the right hand side of the bore section, whilst having areas of low triaxiality comparable to that at the facet sites, has very low normalised resolved shear stress. This reinforces the importance of the hard-soft grain combination and the role of slip in the soft grain in dwell facet nucleation and demonstrates why triaxiality in its own right is not a good indicator of propensity for facet nucleation. We note that all disc facet locations are located in regions where the normalised resolved shear stress is 1.0 or higher, indicating that slip on softly orientated grains is a prerequisite for facet nucleation. Disc facet sites are found to cluster in the region of high resolved shear stress. So far, the role of dwell and load shedding in relation to the observed facet sites has not been addressed, and this is the crucial aspect of this study and is addressed next.

4.1. Assessment of soft-hard grain stress state, slip, and load shedding at disc facet sites

The oligocrystal sub-models subjected to the appropriate stress state dwell loading at each of the disc facet sites are utilised in order to extract out the peak values of hard-grain basal stress at the end of the dwell period (as demonstrated and developed in

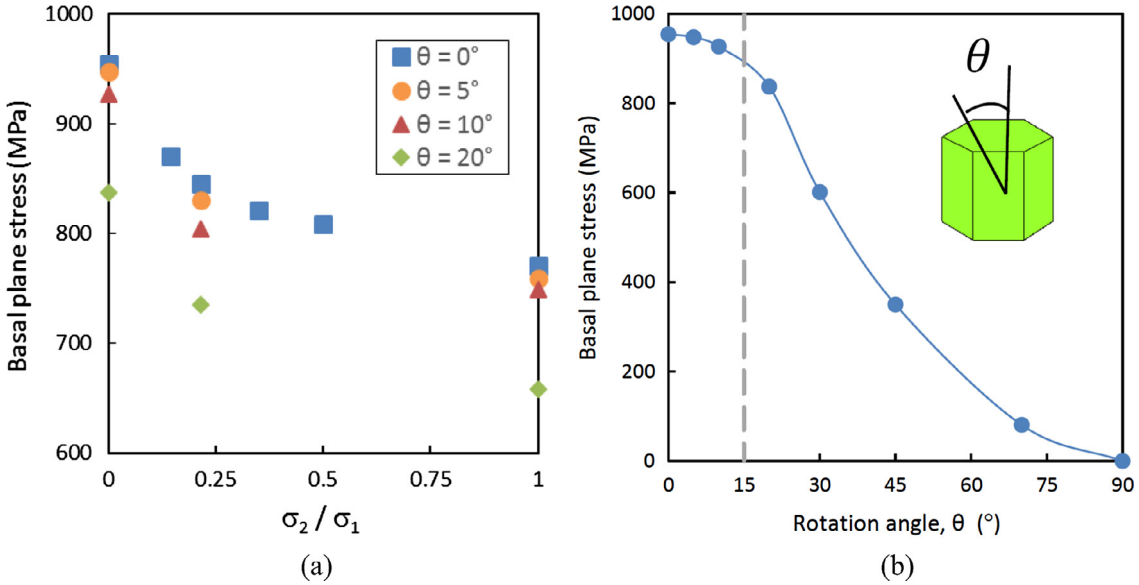

Fig. 12. Hard grain orientation and stress state effect for (a) biaxial loading and, (b) crystal c-axis parallel with principal uniaxial stress loading.

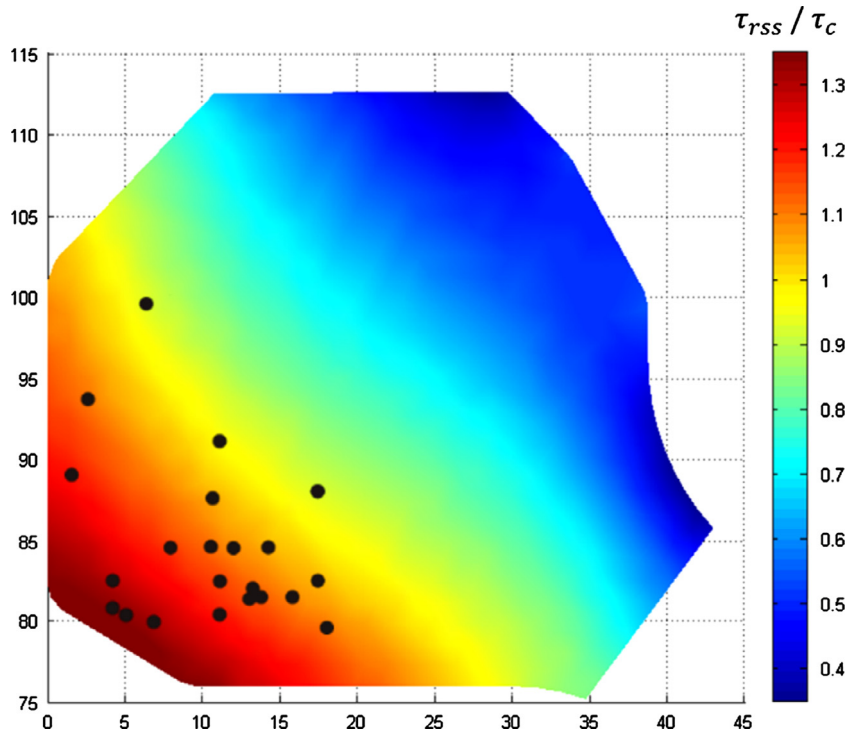

Fig. 14. Normalised resolved shear stresses at the experimentally observed facet sites (and calculated everywhere with respect to a soft grain prism slip system) for the disc bore section.

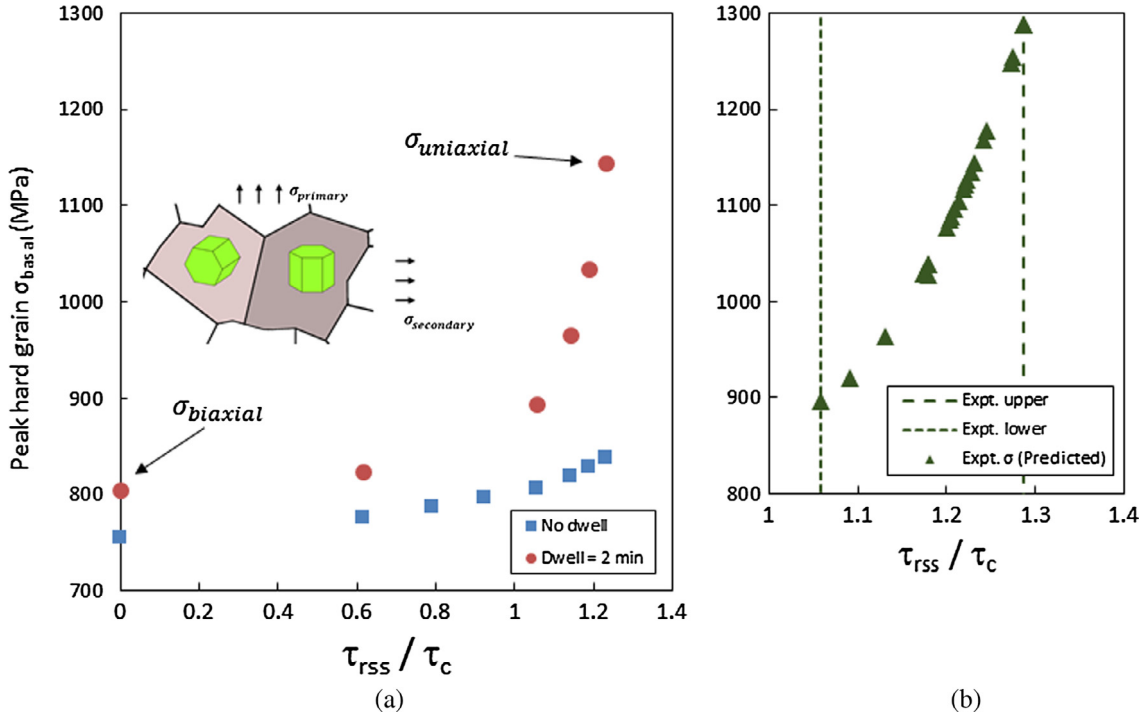

Fig. 15. Peak hard-grain stresses versus normalised resolved shear stress (a) from sub-model crystal plasticity study, and (b) predicted facet site stress state, as interpolated from (a).

Fig. 9). During the dwell, load shedding potentially occurs (depending on the stress state and hence the soft grain prism system resolved shear stress). Peak hard-grain basal stresses are plotted against the associated normalised shear stress for the site-specific load history (which Fig. 14 shows to be equivalent to stress state) as shown in Fig. 15(a) for loading conditions in which dwell is both included and excluded.

Firstly, the graph in Fig. 15(a) shows again the role of the biaxiality stress state, or equivalently, the soft-grain prism system resolved shear stress on the resulting hard-grain basal stresses.

Table 2
Predicted disc hard-grain basal stresses for disc facet sites from CPFE model.

Facet number	τ_{rss}/τ_c	Predicted expt. σ (MPa)	Facet number	τ_{rss}/τ_c	Predicted expt. σ (MPa)
a1	1.180	1027	a14	1.231	1144
a2	1.185	1039	a15	1.209	1097
a3	1.213	1105	a16	1.272	1249
a4	1.227	1135	a17	1.286	1287
a5	1.131	963	a18	1.174	1029
a6	1.286	1287	a19	1.272	1249
a7	1.274	1254	a20	1.286	1287
a8	1.199	1076	a21	1.174	1029
a9	1.221	1122	a22	1.091	920
a10	1.180	1039	a23	1.205	1088
a11	1.223	1126	a24	1.245	1177
a12	1.241	1168	a25	1.219	1118
a13	1.058	896	a26	1.203	1084

More significantly, it makes very clear that the inclusion of the dwell leads to very strong stress redistribution and load shedding, pushing up the hard-grain basal stresses greatly. The magnitude of the load shedding, interestingly, is also seen to be dependent on the stress state (and hence equivalently, the resolved shear stress). The increase in basal stress in the hard grain, due to load shedding, is observed to be ~350 MPa after dwell for a uniaxial stress state, but less than 50 MPa for the equibiaxial loading case.

The results in Fig. 15(a) allow us to examine the load shedding and the hard-grain basal stresses at the disc sites at which facets are known to nucleate. With use of the map in Fig. 14, the prism system resolved shear stresses at each disc facet site are extracted and combined with the results of Fig. 15(a) in order to establish the peak basal stresses after load shedding at each facet site. These are shown in Fig. 15(b) against the disc facet site resolved shear stress. This is reproduced in tabular format in Table 2.

We note that the majority of facet sites cluster around a peak basal stress of 1100–1150 MPa with some outliers on either side, both higher and lower, and are close to an approximate value for the c-axis tensile strength of titanium (~1200 MPa) [32]. This strength is quoted as a useful figure which provides a bound on our analyses; as it shows that the peak basal stresses are in a region close to the approximate tensile strength.

A clear message from these results is that the disc facet nucleation sites are in locations for which high resolved shear stresses exist on the soft grain of the hard-soft combination, for which considerable load shedding occurs, significantly pushing up the hard-grain basal stresses. In summary, all the disc facet locations generate high load shedding and high basal stresses. The primary significance of this is that load shedding is an essential factor in identifying those disc locations where faceting is observed (where also, the hard-soft grain combination also has to exist). This provides persuasive evidence that facet nucleation in discs is caused by load shedding; what is clear is that were the load shedding not to occur, the stresses at the facet sites would remain unremarkable.

The results also provide persuasive evidence that the rogue, or hard-soft grain combination, with respect to the primary (hoop) loading, is also an essential feature of facet formation in discs. Finally, it is also clear that the stress state local to the hard-soft grain combination is also a key factor in facet nucleation, since it determines the magnitude of the resolved shear stress on the soft grain prism system, thus determining the slip activation and hence the load shedding during dwell. A uniaxial stress state at the microstructure level transpires as a result to be more damaging than a biaxial (or more generally triaxial) stress state.

We have presented a multi-scale linkage of the details of microstructure using crystal plasticity (which is the scale that must be considered for cold dwell) right up to the component in-service stress scale relevant to aero-engines in operation. A methodology has been established which potentially provides a strong criterion for dwell failure. The macroscale operating stresses of the discs are far below macroscopic yield stresses, and discs may be adequately and appropriately modelled using elastic analyses. With knowledge of the hard-soft grain combination, resolved shear stresses for any location in the disc geometry may be extracted (assuming a rogue grain combination is present) from which we can ultimately infer likely hard grain basal stresses, which provides the criterion for failure.

5. Conclusions

This paper establishes the link between disc component level testing and crystal plasticity finite element modelling, in the context of cold dwell fatigue. Furthermore this paper has presented a detailed examination of the contribution of load shedding to facet nucleation in dwell fatigue in compressor disc geometries through investigation of the local stress state at the rogue grain combination and how it relates to the macroscopically applied boundary conditions.

The hard grain orientation with respect to the stress state is a key requirement for faceting; misalignment of up to 15° with the principal tensile loading axis shows equivalent basal stresses whereas with further deviation from the principal tensile axis, the stress on the basal plane drops off significantly. This explains why most facets observed in dwell fatigue experiments have been found to be orientated to the principal loading direction within ±15°.

The role of the biaxial remote stress state on the rogue pair has been investigated, and results have been found to be commensurate with the findings of Doquet and DeGreef [8], who hypothesise that biaxiality may have an ameliorating effect on fatigue life (with the caveat of a limited experimental dataset). The detailed micro-level study presented here provides the mechanistic basis for this phenomenon.

The disc component facet observations together with the crystal plasticity sub-model oligocrystal approach provide persuasive evidence that a hard-soft grain combination is required for facet formation, that the remote stress state influences the resolved shear stress on the soft grain initiating slip (with uniaxial stress state more damaging than biaxial), and that the load shedding which results is essential in pushing up the hard-grain basal stress to nucleate facets. The absence of any one of the rogue grain combination, the stress state, or the load shedding renders the observed disc facet locations unexplainable. However, together, they provide a persuasive mechanistic basis and quantitatively predictive methodology for facet nucleation in aero-engine discs.

Acknowledgements

The authors wish to acknowledge input and perspectives from Prof David Rugg, Dr Adrian Walker, and Dr Kate Fox at Rolls-Royce plc. We wish to thank Dr Zhen Zhang, Imperial College, for helpful discussions.

MC and FPED gratefully acknowledge financial support from Rolls-Royce plc and from the Engineering and Physical Sciences Research Council funded *HexMat* programme grant EP/K034332/1 (http://www.imperial.ac.uk/hexmat). FPED acknowledges Royal Academy of Engineering/Rolls-Royce research chair funding.

References

[1] Lütjering G, Williams JJC. Titanium. Springer; 2007.
[2] Rugg D, Dixon M, Dunne FP. Effective structural unit size in titanium alloys. J Strain Anal Eng Des 2007;42(4):269–79.
[3] Stroh AN. The formation of cracks as a result of plastic flow. Proc R Soc Lond Ser Math Phys Sci 1954;223(1154):404–14.
[4] Evans WJ, Bache MR. Dwell-sensitive fatigue under biaxial loads in the near-alpha titanium alloy IMI685. Int J Fatigue 1994;16(7):443–52.
[5] Hasija V, Ghosh S, Mills MJ, Joseph DS. Deformation and creep modeling in polycrystalline Ti–6Al alloys. Acta Mater 2003;51(15):4533–49.
[6] Dunne FPE, Rugg D. On the mechanisms of fatigue facet nucleation in titanium alloys. Fatigue Fract Eng Mater Struct 2008;31(11):949–58.
[7] Anahid M, Samal MK, Ghosh S. Dwell fatigue crack nucleation model based on crystal plasticity finite element simulations of polycrystalline titanium alloys. J Mech Phys Solids 2011;59(10):2157–76.
[8] Doquet V, De Greef V. Dwell-fatigue of a titanium alloy at room temperature under uniaxial or biaxial tension. Int J Fatigue 2012;38:118–29.
[9] Bonnand V, Chaboche JL, Gomez P, Kanouté P, Pacou D. Investigation of multiaxial fatigue in the context of turboengine disc applications. Int J Fatigue 2011;33(8):1006–16.
[10] Kallmeyer AR, Krgo A, Kurath P. Evaluation of multiaxial fatigue life prediction methodologies for Ti-6Al-4V. J Eng Mater Technol 2002;124(2):229–37.
[11] Rice JR, Tracey DM. On the ductile enlargement of voids in triaxial stress fields*. J Mech Phys Solids 1969;17(3):201–17.
[12] Helbert AL, Feaugas X, Clavel M. The influence of stress trlaxiality on the damage mechanisms in an equiaxedα/β Ti-6Al-4V alloy. Metall Mater Trans A 1996;27(10):3043–58.
[13] Kumar J, Srivathsa B, Kumar V. Stress triaxiality effect on fracture behavior of IMI-834 titanium alloy: a micromechanics approach. Mater Des 2009;30(4):1118–23.
[14] Lefranc P, Doquet V, Gerland M, Sarrazin-Baudoux C. Nucleation of cracks from shear-induced cavities in an α/β titanium alloy in fatigue, room-temperature creep and dwell-fatigue. Acta Mater 2008;56(16):4450–7.
[15] Gerland M, Lefranc P, Doquet V, Sarrazin-Baudoux C. Deformation and damage mechanisms in an α/β 6242 Ti alloy in fatigue, dwell-fatigue and creep at room temperature. Influence of internal hydrogen. Mater Sci Eng A 2009;507(1–2):132–43.
[16] Dunne FPE, Walker A, Rugg D. A systematic study of hcp crystal orientation and morphology effects in polycrystal deformation and fatigue. Proc R Soc Math Phys Eng Sci 2007;463(2082):1467–89.
[17] Bache MR, Dunne FPE, Madrigal C. Experimental and crystal plasticity studies of deformation and crack nucleation in a titanium alloy. J Strain Anal Eng Des 2010;45(5):391–9.
[18] Pilchak AL, Williams JC. Observations of facet formation in near-α titanium and comments on the role of hydrogen. Metall Mater Trans A 2010;42(4):1000–27.
[19] Zhang Z, Cuddihy MA, Dunne FPE. On rate-dependent polycrystal deformation: the temperature sensitivity of cold dwell fatigue. Proc R Soc A 2015;471(2181).
[20] ASTM International <www.astm.org/Standards/E837.htm>, 'Standard Test Method for Determining Residual Stresses by the Hole-Drilling Strain Gage Method'; 2013.
[21] Dye D, Roder B, Tin S, Rist M, James J, Daymond M. Modeling and measurement of residual stresses in a forged IN718 superalloy disc. Superalloys 2004;2004:315–22.
[22] Dunne FPE, Rugg D, Walker A. Length scale-dependent, elastically anisotropic, physically-based hcp crystal plasticity: application to cold-dwell fatigue in Ti alloys. Int J Plast 2007;23(6):1061–83.
[23] Lee EH. Elastic-plastic deformation at finite strains. J Appl Mech 1969;36(1):1–6.
[24] Littlewood PD, Wilkinson AJ. Local deformation patterns in Ti–6Al–4V under tensile, fatigue and dwell fatigue loading. Int J Fatigue 2012;43:111–9.
[25] Jiang J, Britton TB, Wilkinson AJ. The orientation and strain dependence of dislocation structure evolution in monotonically deformed polycrystalline copper. Int J Plast 2015;69:102–17.
[26] Gong J, Benjamin Britton T, Cuddihy MA, Dunne FPE, Wilkinson AJ. ⟨a⟩ Prismatic, ⟨a⟩ basal, and ⟨c+a⟩ slip strengths of commercially pure Zr by micro-cantilever tests. Acta Mater 2015;96:249–57.
[27] Liang H, Dunne FPE. GND accumulation in bi-crystal deformation: crystal plasticity analysis and comparison with experiments. Int J Mech Sci 2009;51(4):326–33.
[28] Gong J, Wilkinson AJ. Anisotropy in the plastic flow properties of single-crystal α titanium determined from micro-cantilever beams. Acta Mater 2009;57(19):5693–705.
[29] Conrad H. Thermally activated deformation of α titanium below 0.4 TM. Can J Phys 1967;45(2):581–90.
[30] Sauzay M, Liu J, Rachdi F, Signor L, Ghidossi T, Villechaise P. Physically-based simulations of the cyclic behavior of FCC polycrystals. Adv Mat Res 2014:891–2.
[31] Sinha V, Spowart JE, Mills MJ, Williams JC. Observations on the faceted initiation site in the dwell-fatigue tested Ti-6242 alloy: crystallographic orientation and size effects. Metall Mater Trans A 2006;37A(5):1507–18.
[32] Jones IP, Hutchinson WB. Stress-state dependence of slip in Titanium-6Al-4V and other H.C.P. metals. Acta Metall 1981;29(6):951–68.